EXPERIMENTAL STUDY OF PULSATIONS IN THE FORWARD SEPARATION ZONE IN A SUPERSONIC FLOW

V. I. Zapryagaev and S. G. Mironov

UDC 534.13:533.601.15

The need to study pulsation phenomena for configurations with forward separation zones stems from the possibility of reducing the resistance of a body by appropriately choosing the geometry of these zones. Data on the averaged and fluctuation characteristics of bodies with a spike tip was reported in [1-15]. Fluctuations in a separation zone [6, 8] are divided into pulsations for which there is and is not a significant change in the zone. Fluctuations of the first type have been referred to collectively as a transient second-order regime [6] and as pulsations [8], E-type pulsations [4] or catastrophic pulsations [5]. Mass rate pulsations are among these types of fluctuations [13-15]. Fluctuations for which there is no appreciable change in the separation zone are collectively termed a transient first-order regime [6] or oscillations [8]. The authors of [10-12] used the term spike noise and did not separate the pulsations into two types.

To expedite our discussion and reduce the number of terms, here we adopt the names mass-rate pulsations and acoustic oscillations to distinguish the types of fluctuations. These terms are consistent with the terminology used in the works cited above. We present experimental data on the magnitude of the pressure pulsations and the discrete-tone frequencies for a model with a forward separation zone of variable geometry. Results are presented from a combined analysis of the motion of shock waves ahead of a cylinder with a spike and pressure pulsations on the end of the cylinder. The mechanism of the pulsations is discussed, and a criterion is obtained for relative mass transfer during pulsations in the separation zone.

1. Experiments were conducted on an axisymmetric model with a zero angle of attack. The model was a cylinder of the diameter D = 80 mm. A holder 16 mm in diameter was affixed and moved coaxially inside the cylinder. A conical tip with a half-angle of 20° was secured to the end of the holder to form a spike-tipped body. A variant employed here was the installation of a cone on the holder, the diameter of the base of the cone d = 40 or 60 mm

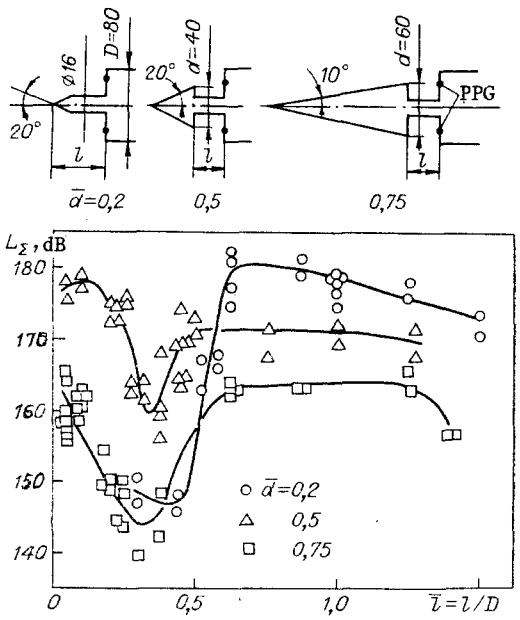

Fig. 1

Novosibirsk. Translated from Zhurnal Prikladnoi Mekhaniki i Tekhnicheskoi Fiziki, No. 4, pp. 116-124, July-August, 1989. Original article submitted October 29, 1987; revision submitted March 1, 1988.

 0021-8944/89/3004-0620$12.50

(diagram in Fig. 1). Two pressure-pulsation gauges (PPG) were placed on the back end of the cylinder 25 mm from the center of the end. The gauges were secured to the model in vibration-resistant housings. The length ℓ of the holder could be changed within the range 0-120 mm. Tests were conducted in a supersonic wind tunnel [16] with the flow Mach number $M_\infty = 2.04$ and the Reynolds number $Re_\infty = 2.4 \cdot 10^6$. The Reynolds number was calculated on the basis of the diameter of the cylinder and the parameters in the incoming flow.

The signals from the gauges were sent to preamplifiers and were recorded on a multichannel magnetograph N067. Subsequent analysis of the signals produced frequency spectra. Spectral analysis was performed with an SK4-56 analyzer operated together with an N306 two-coordinate recorder. The rms value of the signal in the band 20-20,000 Hz was measured with a V3-57 microvoltmeter designed to measure noise signals. The amplitude–frequency characteristic of the piezoelectric pressure gauges was checked by comparison with the readings of an MK-6 condenser microphone. The gauges were calibrated with a PP101A pistophone. The error of measurement of the amplitude of the pulsations was estimated to have been 2 dB.

We used an IAB-451 shadowgraph with an annular knife to obtain instantaneous Schlieren photographs of the flow pattern. This allowed us to record the density gradient in all directions. The light source was an ISh-5 strobe light with an illumination time of about 1 μsec. The scheme of formation of the pulses for the illumination of the lamp was such as to permit coupling of the flow field with the phase of the observed pressure pulsations [17]. This approach makes it possible to obtain oscillograms whose initial moment corresponds to the moment of flashing of the light.

2. Figure 1 shows the dependence of the overall level of the pressure pulsations L_Σ on the relative length $\bar{\ell} = \ell/D$ for three configurations of the separation zone. The maximum levels correspond to the spiked cylinder ($\bar{d} = d/D = 0.2$) and reach 182 dB. The pulsations are small ($L_\Sigma \approx 147$ dB) when the spike is shorter than the distance to the shock wave in front of the cylinder. Approach of the tip of the spike to the wave leads to a substantial increase in pulsations. The distance $\bar{\ell}_s$ from the end of the cylinder to the shock wave, measured from a Schlieren photograph with $\bar{\ell} < \bar{\ell}_s$, is equal to 0.45. The dependence of L_Σ on $\bar{\ell}$ for cones with $\bar{d} = 0.5$ and 0.75 clearly shows a reduction in L_Σ by 10-12 dB at $\bar{\ell} \approx 0.35$.

The frequency of the discrete tone was determined from the peaks seen on the spectrograms. Figure 2a-c shows the dependence of the Strouhal number $Sh = f\ell/u_\infty$ on $\bar{\ell}$ for $\bar{d} = 0.2$, 0.5, and 0.75. The dark points correspond to the observed magnitude of the pulsations (the maximum peak on the spectrogram). Figure 3 shows several spectrograms for the characteristic pulsation regimes. The quantity p_f is the level of fluctuation pressure at a frequency f equal to 200 Hz in the band. The light points show the positions of the lower-amplitude peaks on the frequency axis. Whether or not these peaks are detected against the noise background depends on the moment of recording and the number of the pressure gauge. The several branches of the relation $Sh(\bar{\ell})$ correspond to modes of oscillation n = 1, 2, ... The nine characteristic regimes corresponding to those in Table 1 are indicated at the top of the figure. The absence of points in Fig. 2 at $\bar{\ell} < 0.6$ for $\bar{d} = 0.2$ and $\bar{\ell} < 0.35$ for $\bar{d} = 0.75$ in the present study is due to the noisy character of the signal. No discrete frequencies were discernible in this case. The dependence of Sh on $\bar{\ell}$ for $\bar{d} = 0.2$ and 0.5 consists of two sections: an increase in Sh with an increase in $\bar{\ell}$; relative constancy of Sh with a change in $\bar{\ell}$. At $\bar{\ell} > 1$, $\bar{d} = 0.2$ and 0.5 for the first three modes of oscillation, Sh takes values close to 0.3, 0.55, 0.86. For $\bar{d} = 0.75$, the scatter of the points relative to these values

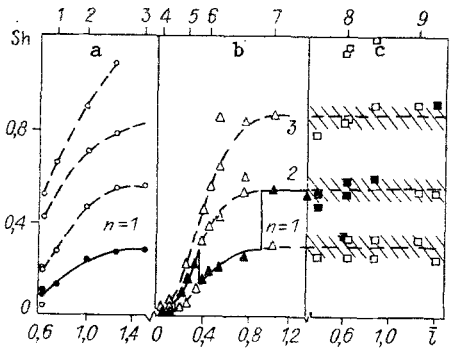

Fig. 2

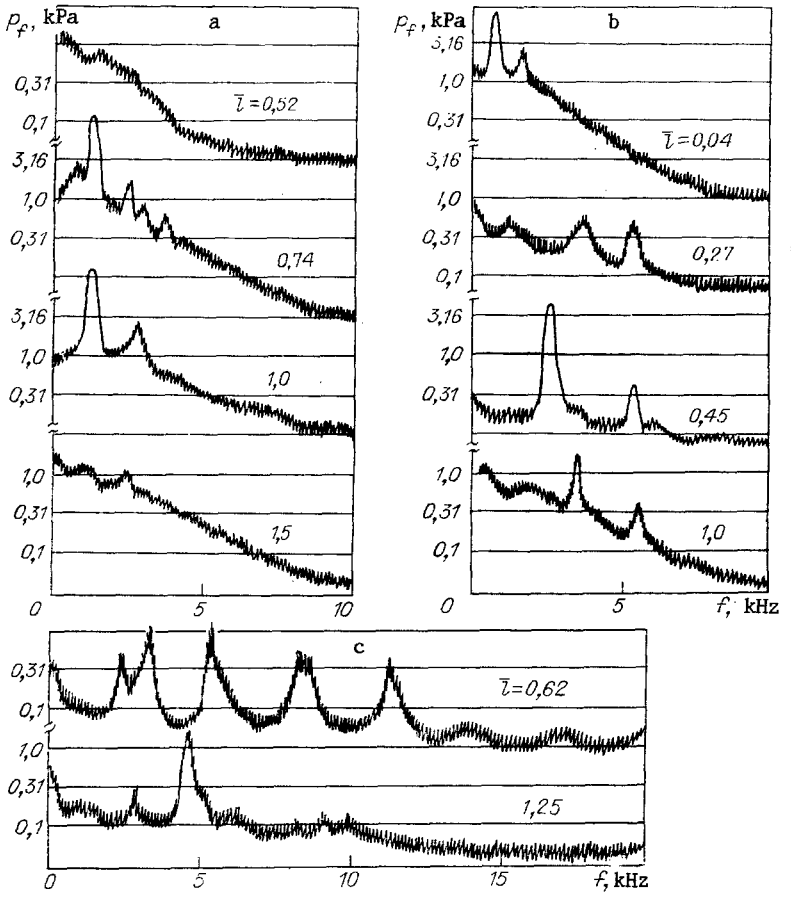

Fig. 3

TABLE 1

No. of regime	$\bar{d}$	$\bar{l}$	f, kHz	p_f, kPa	Sh	ρ_0, kg/m^3	$\bar{p}$	$\bar{\Delta}$
1	0,2	0,74	1,14	12,5	0,135	1,73	0,067	0,56
2	0,2	1,0	1,54	14,0	0,244	1,73	0,076	0,36
3	0,2	1,5	1,0	1,5	0,271	0,57	0,025	0,1
4	0,5	0,04	0,71	9,0	0,046	1,73	0,049	0,92
5	0,5	0,27	1,28	0,6	0,054	1,02	0,0005	0,009
6	0,5	0,45	2,67	5,0	0,19	0,96	0,049	0,27
7	0,5	1,0	3,41	2,0	0,54	0,53	0,035	0,07
8	0,75	0,62	3,4	1,0	0,34	0,44	0,021	0,06
9	0,75	1,25	4,5	1,7	0,89	0,35	0,045	0,05

is substantial but most of the measured frequencies lie within the range $\Delta Sh = \pm 0.06$ (see Fig. 2). The aggregate of the data in [18] gives values of Sh close to these values. The independence of Sh of $\bar{l}$ proportionally decreases the frequencies with an increase in the longitudinal dimension of the separation zone. The following relation was presented in [19] for pulsations in shear flows in the presence of the characteristic dimension

$$l/u_1 + l/u_2 = n/f, \tag{2.1}$$

where u_1 is the velocity of longitudinal perturbations in the shear layer (convective velocity); u_2 is the velocity of perturbations in the separation zone upflow. Taking (2.1) into account, we obtain

$$\mathrm{Sh} = nu_1u_2/[u_\infty(u_1 + u_2)]. \tag{2.2}$$

The fact that Sh is independent of $\bar{l}$ means that u_1 and u_2 are independent of $\bar{l}$. The change in Sh seen in Fig. 2 evidently indicates either that there is a significant change in the velocity of the perturbations or that another oscillation mechanism is active for the given $\bar{l}$. For $\bar{d}$ = 0.2 (cylinder with a spike), this change in the relation is seen at $\bar{l}$ = 1.25.

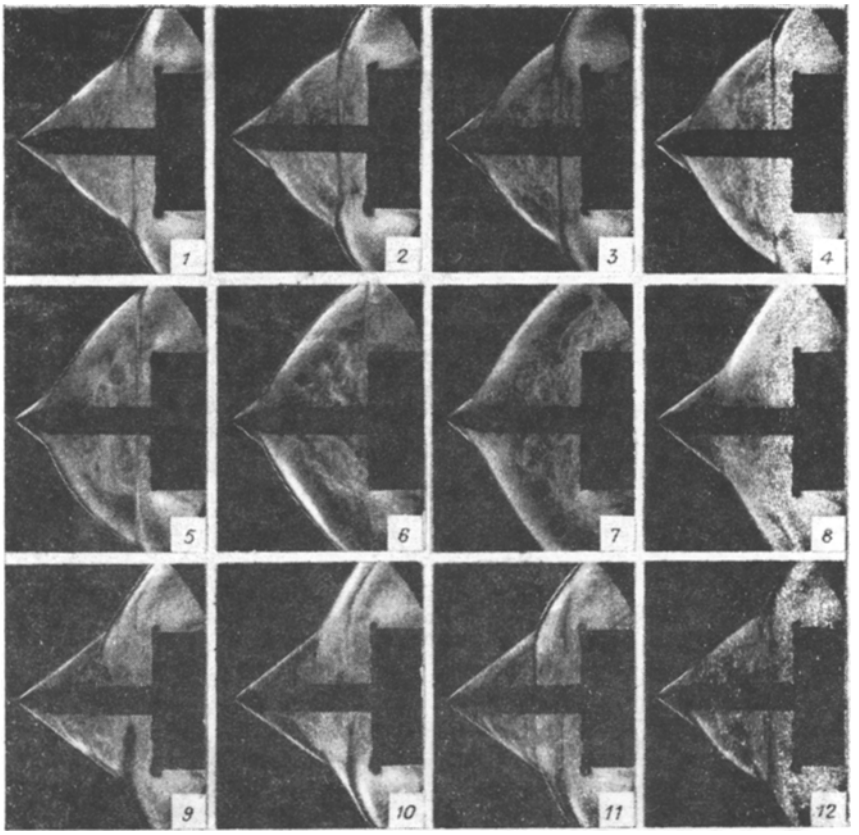

Fig. 4

For $\bar{d} = 0.5$, it is seen at $\bar{\ell} = 0.75$. Considering the previously noted change in the type of pulsations [6, 8], it can be suggested that the change in the dependence of Sh on $\bar{\ell}$ is due to a transition from the mass-rate mechanism of oscillation to oscillations taking place in the opening. The frequency of the latter can be evaluated from (2.1).

The Schlieren photographs (Fig. 4) correspond to different phases of the pulsation process and were obtained by the method described in [17]. The numbers on the characteristic oscillogram of the pressure pulsations $\delta p(\tau)$ (Fig. 5a) denote the moments of time at which the photographs were taken. The time in fractions of the period $\tau = t/T_0$ is plotted off the x axis. The data in Figs. 4 and 5 correspond to $\bar{\ell} = 1.0$. The form of the oscillograms indicates the presence of a random component in the signal. This is manifest in the fact that the oscillatory process is not strictly periodic. For this regime, the rms deviation of the period of oscillation from the mean is 3.5%. In accordance with the terminology used in [20], such a signal can be represented as the sum of deterministic and random signals.

Figure 5b shows the time dependence of the positions of characteristic elements of the wave structure. As such elements, we took the ternary configurations of the shock waves T. The important role of these configurations in the development of the nonsteady process was noted in [21]. Here, $\Delta\ell$ and $\Delta\ell_0$ (points I and II) are the distance from the end of the cylinder to the triple point and from the end to the second shock wave. The presence of two triple points T and two corresponding branches of the relation $\Delta\bar{\ell}(\tau)$ (curves 1 and 2 in Fig. 5b) is probably due to the fact that two adjacent oscillation peaks fell within the field of view of the shadowgraph. This hypothesis allows us to extrapolate curve 1 to the next cycle by means of curve 2. It also follows from the periodicity of the process that curve 3 appears in the second cycle (τ = 1-2), this curve being the analog of curve 1 (4 denotes the position of the secondary shock wave in relation to time). The error of determination of the phase of the oscillatory process was estimated to be $0.03T_0$ and was due mainly to the random component of the signal.

3. The motion of the ternary configurations of the shock waves relative to the pressure oscillations is shown in Fig. 5b, which allows us to clearly describe the oscillatory process. We took the time corresponding to the maximum pressure at the measurement point on the end of the cylinder as the beginning of the count $\tau = 0$. A ternary configuration develops at

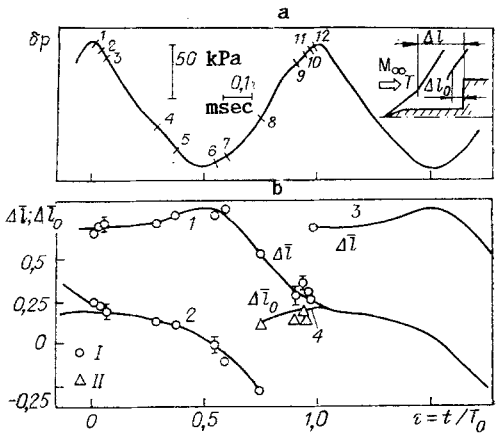

Fig. 5

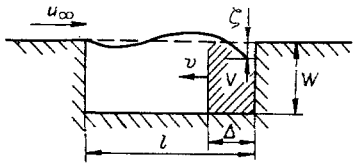

Fig. 6

this moment on the attached conical end of the shock wave near the tip of the spike. The approach, to the tip, of a compression wave propagating counter to the flow in the separation region is responsible for this configuration. During the period of time τ = 0-0.5, the intensity of the curvilinear shock wave increases behind the ternary configuration. This, in turn, leads to an increase in the angle of its inclination and to some forward movement. Here, $\Delta\bar{\ell}$ = 0.8 (photographs 5-7 in Fig. 4). With a spike length $\bar{\ell}$ = 0.75, the intensity of the shock increases so much that the triple configuration disappears and a separated shock wave is formed ahead of the spike tip. The increase in the intensity of the shock is due, in our opinion, to an increase in the intensity of the approaching compression wave.

The transverse dimensions of the separation zone increase, which leads to the displacement of flow-spreading points from the axis and their departure from the end of the cylinder. The latter is manifest in the absence, at this moment of time, of the dark spot visible in Schlieren photographs 1-4 near the outer edge of the end. This spot is interpreted as a region of large density gradients which develops as the flow moves over the end from the axis [22]. The departure of the spreading points from the end interrupts the entry of gas into the separation region and marks the beginning of emptying of this zone. The latter entails a reduction in pressure behind the curvilinear shock wave and causes the ternary configuration to be entrained downflow at velocities up to 180 m/sec. The entrainment velocity was calculated from the relation $\Delta\bar{\ell}(\tau)$ (curve 1 in Fig. 5b) in the interval τ = 0.5-0.75. The velocity of the shock found from the empirical formula in [7] is 154 m/sec. The interval τ = 0.5-0.75 corresponds to emptying of the front separation zone and a decrease in its volume. Transverse contraction of the zone leads to inward deflection of the shear layer and the beginning of interaction with the end of the cylinder. The latter, in turn, leads to the appearance of a separated secondary shock at the distance $\Delta\bar{\ell}_0$ from the end. The formation of this shock is due to stagnation of the flow.

A compression wave is formed in the separation zone simultaneously with the appearance of the secondary shock. The compression wave propagates toward the tip, and thus closes the feedback loop in the oscillatory process. The formation of the shock in front of the end of the cylinder in [7] can be attributed to the supersonic flow velocity behind the main attached shock for the given stage of pulsations. Displacement of the shear layer toward the axis causes streams that are under higher pressure to flow toward the end of the cylinder. This then increases the intensity of the separated shock wave and moves it somewhat farther from the end (curve 4 in Fig. 5b). At τ = 1.0, the downflow-moving system of shock waves interacts with the separated secondary shock (merging of curves 1 and 4 in Fig. 5b – photographs 1 and 12). The interaction is also manifest in a reduction in the velocity of the triple point (τ = 1.0-1.2 in Fig. 5b). The resulting perturbation is displaced downflow and leaves the field of view of the shadowgraph. It is evident from photographs 5-7 how this disturbance moves past the end of the cylinder. As was hypothesized above, the two ternary configurations of shock waves seen in photographs 1-5 correspond to adjacent oscillatory peaks. The asymmetry of the shocks is evident in photographs 9 and 10, this asymmetry having been attributed in [5, 12] to the presence of a rotational mode of oscillation.

The representation on the kinematics of the pulsation process allows us to evaluate the pressure change on the end of the cylinder. The minimum pressure on the end corresponds to the pressure behind the curvilinear shock on the fluid cone that is the external boundary

of the separation region (τ = 0.6, photograph 6). The angle of inclination of the shock decreases from the maximum value near the triple point with an increase in the distance from the axis. To make an evaluation, we take the angle of inclination of the shock to the flow direction at the distance equal to the radius of the cylinder (the measured value of the angle is 57°). The parameters of the incoming flow are known: $M_\infty = 2.04$, $p_\infty = 2.36 \cdot 10^4$ Pa. According to [23], the pressure on the fluid cone $p_1 = 8.63 \cdot 10^4$ Pa. In keeping with the flow scheme, the maximum pressure on the end corresponds to the total pressure for the stream passing through the conical attached shock and the reflected shock. The latter shock originates from the triple point in the direction of the axis (τ = 0.95, photograph 9). The attached shock has an angle of 37°, with $M_1 = 1.724$. The total pressure is $1.92 \cdot 10^5$ Pa (the pressure losses for the oblique shock were considered). To evaluate the intensity of the reflected shock, allowance should be made for its velocity. This was taken equal to the velocity of the triple point. The velocity of the flow behind the oblique shock is 461 m/sec, while the velocity of the reflected shock is 180 m/sec. The difference between these velocities, referred to the local sonic velocity behind the oblique shock, gives the relative Mach number in front of the reflected shock M = 1.05 (the moving reflected shock is more properly referred to as a shock wave). The coefficient which expresses the reestablishment of total pressure is 0.9994 for a direct shock of such intensity, while it is closer to unity for an oblique shock. Thus, the total pressure in the stream passing through the system of two shocks $p_{02} = 1.92 \cdot 10^5$ Pa. The difference between the maximum and minimum pressures gives the theoretical value of the range of pressure pulsations on the end of the cylinder $p_{02} - p_1 = 1.06 \cdot 10^5$ Pa. Comparison with the measured value $1.17 \cdot 10^5$ Pa (Fig. 5) indicates the satisfactory agreement.

The average pressure on the end $(p_{02} + p_1)/2 = 1.39 \cdot 10^5$ Pa is close to the total pressure behind the direct shock ($p_{0dr} = 1.38 \cdot 10^5$ Pa for $M_\infty = 2.04$), which in turn corresponds to the measured average pressures from [15].

4. The representations on the pulsation mechanism in forward separation zones obtained from analysis of the literature and the experimental data described here make it possible to find criterional estimates that will assist in classifying oscillations. As the determining criterion, it is most expedient to introduce the mass of the gas δm participating in the pulsative process in relation to the entire mass of gas in the separation zone m_0. We will call mass-rate pulsations those for which $\delta m/m_0 \sim 1$, while acoustic oscillations will be considered those for which $\delta m/m_0 \ll 1$ is valid.

Let us examine an opening of the length ℓ, depth W, and width S washed by a flow with the velocity u_∞. Oscillations of the shear layer relative to the dividing streamline (which makes sense only for averaged flow) are accompanied by pulsative mass exchange near the back edge of the opening (Fig. 6). We will assume that the mass of the gas participating in mass exchange with the external flow δm occupies the volume V with the characteristic longitudinal dimension Δ. It follows from the continuity equation that

$$\delta m = WS\left[\frac{\partial}{\partial t}\int_0^{\Delta(t)} \rho(x, t)\, dx\right] \tag{4.1}$$

(ρ is the density of the gas in the opening). Here, the characteristic time of inflow (outflow) $\delta t = T_0/2 = 1/(2f)$. This allows us to evaluate the gas flow rate as

$$g = \delta m/\delta t = (WS\Delta\rho_0)/\delta t = 2\rho_0 WS\Delta f. \tag{4.2}$$

On the other hand, differentiation of (4.1) gives us

$$g = WS\left[\int_0^{\Delta} \frac{\partial \rho}{\partial t}\, dx + \rho(\Delta, t)\frac{\partial \Delta}{\partial t}\right] \simeq WS\left[\frac{4\sqrt{2}\, p_f f \Delta}{c_0^2} + \rho_0 v\right]. \tag{4.3}$$

In (4.2) and (4.3), we took $\rho = \rho_0$ (ρ_0 is the time-averaged density). Also,

$$v = \frac{\partial \Delta}{\partial t}, \quad \frac{\partial \rho}{\partial t} = \frac{1}{c_0^2}\frac{\partial p}{\partial t} \simeq \frac{1}{c_0^2}\frac{2\sqrt{2}\,p_f}{\delta t} = \frac{4\sqrt{2}\,p_f f}{c_0^2}$$

(c_0 is the speed of sound in the opening).

We will assume that the inflowing gas forms a plane fluid piston whose velocity is equal to the acoustic velocity v of the compression wave it generates. The connection between v and p in the plane acoustic wave is given by the relation

$$v = p/\rho_0 c_0. \tag{4.4}$$

Comparing (4.2) and (4.3) with allowance for (4.4), we obtain an expression for the size of the mass-transfer region

$$\Delta = \sqrt{2}\,p_f c_0/[(\rho_0 c_0^2 - 2\sqrt{2}\,p_f) f]. \tag{4.5}$$

Changing over to dimensionless variables in (4.5), we obtain a relation for the criterion $\bar{\Delta}$, which characterizes mass exchange with oscillations in the cavity:

$$\bar{\Delta} = \left(1 + r\frac{\gamma - 1}{2}M_\infty^2\right)^{1/2}\bar{p}/[2M_\infty \mathrm{Sh}(1 - \bar{p})], \tag{4.6}$$

where $\bar{p} = 2\sqrt{2}p_f/(\rho_0 c_0^2)$; $\bar{\Delta} = \Delta/\ell$; p_f is the pressure corresponding to the pulsation spectrum; γ is the adiabatic exponent. Here, it is understood that the temperature of the gas in the cavity is close to the restitution temperature in the turbulent boundary layer [1] and is determined by the coefficient of restitution r = 0.896.

Table 1 shows values of relative mass transfer $\bar{\Delta}$ for regimes for which discrete components are seen (see Fig. 3) in the pulsation spectrum. The density ρ_0 in the cavity was found from the equation of state. Here, the pressure distribution along the cavity was not considered. For an opening located on a plate or on a cylindrical surface (Fig. 6), pressure in the cavity is close to pressure in the incoming flow but increases near the back end [1]. For a pulsative flow with a spike at $\bar{\ell} \simeq 1$, it is assumed that, in accordance with [6], pressure in the separation zone is close to the pressure behind the direct shock (regimes 1, 2, and 4). It was shown in [6] that, in the case of long spikes, pressure in the separation zone is roughly equal to the pressure on the fluid cone for steady-state flow about the object. Here, the angle is determined from Schlieren photographs taken with a long exposure. The pressure in the conical part of the separation zone was found using the results of calculations of conical flow. We ignored the conicity of the volume of the separation zone. Allowance for this should lead to an increase in $\bar{\Delta}$ for regimes 1, 2, and 4 compared to the data in Table 1. The increased pressure near the back end of the separation zone leads to a decrease in $\bar{\Delta}$ due to the drop in $\bar{p}$ (increase in density near the back end) for regimes 3 and 5-9. For regime 4, we took $\bar{\ell} = 0.5$ as the characteristic length.

According to the above estimates and the data in Fig. 2, regimes 3, 5 and 7-9 ($\bar{\Delta} < 0.1$) should be classed as acoustic oscillations. Regimes 1 and 2 ($\bar{\Delta} \geq 0.56$) should be regarded as mass-rate pulsations. Transient oscillations (strong acoustic or weak mass-rate oscillations) take place in regimes 4 and 6. The notion of separating pulsations into mass-rate and acoustic pulsations with respect to the relative mass transfer that takes place is consistent with the literature division into two types of pulsations.

LITERATURE CITED

1. P. K. Chang, Separation of Flow, Pergamon Press, New York (1970).
2. P. K. Chang, Control of Flow Separation, Halsted Press, New York (1975).
3. C. J. Wood, "Hypersonic flow over spiked cones," J. Fluid Mech., 12, Pt. 4 (1962).
4. Holden, "Experimental study of separated flows at hypersonic velocities. Part 1. Separated flows on axisymmetric spiked bodies," AIAA J., 4, No. 4 (1966).
5. A. Demetriades and A. T. Hopkins, "Asymmetric shock-wave oscillations on spiked bodies of revolution," J. Spacecr. Rockets, 13, No. 11 (1976).
6. A. N. Antonov and V. K. Gretsov, "Study of nonsteady supersonic separated flow about bodies," Izv. Akad. Nauk SSSR, Mekh. Zhidk. Gaza, No. 4 (1974).
7. A. N. Antonov, V. K. Gretsov, and S. P. Shalaev, "Nonsteady supersonic flow about spike-tipped bodies," Izv. Akad. Nauk SSSR, Mekh. Zhidk. Gaza, No. 5 (1976).
8. A. G. Panaras, "Pulsating flows about convex axisymmetric bodies," AIAA J., 19, No. 8 (1981).

9. V. N. Karlovskii and V. I. Sakharov, "Numerical study of supersonic flow about bluff bodies with an extended spike tip," Izv. Akad. Nauk SSSR, Mekh. Zhidk. Gaza, No. 3 (1986).
10. J. S. Shang, W. L. Hankey, and R. E. Smith, "Flow oscillations of spike-tipped bodies," AIAA Paper No. 80-0062, Pasadena, CA (1980).
11. W. L. Hankey and J. S. Shang, "Analysis of self-excited oscillations in fluid flows," AIAA Paper No. 80-1346, Snowmass, CO (1980).
12. W. Calarese and W. L. Hankey, "Modes of shock-wave oscillations on spike-tipped bodies," AIAA J., 23, No. 2 (1985).
13. D. J. Maull, "Hypersonic flow over axially symmetric spiked bodies," J. Fluid Mech., 8, Pt. 4 (1960).
14. B. N. Dan'kov and L. V. Novikov, "Nonsteady supersonic flow about a cone with a disk flap," Izv. Akad. Nauk SSSR, Mekh. Zhidk. Gaza, No. 4 (1968).
15. V. S. Avduevskii, V. K. Gretsov, and K. I. Medvedev, "Stability of flows with forward separation zones," Izv. Akad. Nauk SSSR, Mekh. Zhidk. Gaza, No. 1 (1972).
16. I. I. Volonikhin, V. D. Grigor'ev, V. S. Dem'yanenko, et al., "Supersonic wind tunnel T-313," in: Aerodynamic Investigations [in Russian], Inst. Teor. Prikl. Mekh. Sib. Otd., Akad. Nauk SSSR, Novosibirsk (1972).
17. V. I. Zapryagaev and S. G. Mironov, "Method of correlating flow-field photographs with a measured local parameter," in: Methods of Conducting Aerophysical Studies: Materials of the 4th All-Union Conference on Methods of Conducting Aerophysical Studies, Inst. Teor. Prikl. Mekh., Sib. Otd., Akad. Nauk SSSR, Novosibirsk (1987).
18. V. I. Zapryagaev, "Study of pulsations in the separation region of a free cavity in a supersonic flow," Zh. Prikl. Mekh. Tekh. Fiz., No. 6 (1985).
19. D. Rockwell, "Oscillations of impinging shear layers," AIAA J., 21, No. 5 (1983).
20. J. Bendat and A. G. Piersol, Random Data: Analysis and Measurement Procedures, Wiley, New York (1971).
21. V. G. Dulov and G. A. Luk'yanov, Gasdynamics of Discharge Processes [in Russian], Nauka, Novosibirsk (1984).
22. M. A. Ibragim, A. O. Serov, et al., "Reflection of a plane shock wave from a body with an opening," Izv. Akad. Nauk SSSR, Mekh. Zhidk. Gaza, No. 5 (1985).
23. Yu. A. Kibardin, S. I. Kuznetsov, A. N. Lyubimov, and B. Ya. Shumyatskii, Atlas of Gasdynamic Functions with High Air-Flow Velocities and Temperatures [in Russian], GÉI, Moscow, Leningrad (1961).